2025 6th International Conference on Control and Fault-Tolerant Systems (SysTol)
October 6-8 2025. Ayia Napa, Cyprus

Remaining Useful Life Prediction of Solid Oxide Fuel Cells Using Moving Horizon Estimation

Andrea Caspani, Rudy R. Negenborn and Vasso Reppa

Abstract— **Solid Oxide Fuel Cells are promising power generation technologies, especially for large-scale applications. As the marine industry is targeting a full de-carbonization by year 2050, increasing attention is being directed toward the implementation of these technologies. Solid Oxide Fuel Cells are complex systems where thermodynamics and electrochemical reactions are coupled, resulting in highly non-linear dynamics, tight operational constraints, and multiple distributed sensors. Those quantities that cannot be directly measured, need to be estimated. Among these, the so called Area Specific Resistance is an indicator of cell's health condition, related to the cell degradation. This paper proposes a Moving Horizon Estimator based on an extended state-space model of a methane-fueled Solid Oxide Fuel Cell, to estimate in real time the Area Specific Resistance of the cell. Using the estimated value, along with its maximum and average rates, a predictive framework is developed to estimate the Remaining Useful Life of the cell. Simulations are used to illustrate the application and the efficiency of the proposed method.**

I. Introduction

Solid Oxide Fuel Cells (SOFCs) represent a valuable alternative to conventional power generation systems due to their fuel flexibility and high efficiency. Conversely, SOFCs are complex technologies that operate at extremely high temperatures, require a significant initial investment, and are relatively bulky [1]. These characteristics make them particularly well-suited for the maritime sector, especially considering that the International Maritime Organization (IMO) has set 2050 as the target year for the complete decarbonization of the industry [2].

SOFCs are electrochemical conversion devices that generate electrical power by oxidizing the hydrogen contained in a fuel. There are two main gas flows entering the cell: at the anode, a mixture of fuel gases, and at the cathode, air. The reaction at the electrolyte membrane releases electrons from the fuel and transfers them to the air stream, generating electricity and heat. The complexity in SOFCs arises from the intersection of thermodynamics, and electrochemistry. This complexity is also reflected in the physical realization of the fuel cell, consisting of interconnected system including heat exchangers, afterburners, fans, and pipes, power electronics and current distribution systems. It goes without saying that these systems exhibit non-linear dynamics, operate within strict constraints, and are equipped with several sensors [3].

Department of Maritime and Transport Technology, Faculty of Mechanical Engineering, Delft University of Technology, Mekelweg 2, 2628 CD Delft, the Netherlands. (e-mail: a.caspani@tudelft.nl, r.r.negenborn@tudelft.nl, v.reppa@tudelft.nl)

This research has been performed as part of the project AmmoniaDrive, funded by the NWO Perspectief Programme under Grant no. P20-18/14267. AmmoniaDrive 2022

The main drawbacks that hinder the widespread adoption of SOFCs in industry and in the maritime sector are their limited dynamic performance and degradation. A typical response time of a cell is on the order of minutes, mainly because thermal dynamics is comparatively slow compared to electrical one [4]. On the other hand, the way you operate the cell, can increase its internal degradation and reduce its operational lifetime. The degradation in SOFC is caused by different phenomena, such as thermal stress, membrane poisoning, and other mechanisms, and manifests itself in different ways [5]. One of them is a slow monotonic increase in the area-specific resistance (R_a), which is the internal resistance of the cell, corresponding to loss in electrical efficiency. This phenomenon is called voltage degradation and is closely related to system operating conditions. Recent studies assessed voltage degradation rates ranging from 0.5% to 1.4% per 1,000 hours of operation in steady state [6]. Considering that the expected lifetime of a SOFC stack typically falls between 40,000 and 60,000 hours, this corresponds to a voltage drop of approximately 10% from its initial value under nominal conditions [7], which negatively affects the available power output and system efficiency.

Given the impact of degradation on SOFC performance, assessing the health status of a SOFC is a highly relevant topic for both academia and industry. In [8], the authors developed subsequent Extended and Unscented Kalman Filters to track the cell's R_a and provide a prediction of its remaining useful life (RUL). In this approach, a linear model of R_a drift is used: first, R_a is estimated using a UKF, then an EKF is employed to identify the drift, which is used for RUL prediction. Similarly, a Particle Filter is employed in [9] to monitor the degradation trend of a SOFC operating under constant load conditions, where a linear drift model of R_a is also assumed. A hybrid approach is proposed in [10], combining a lumped dynamic model with real-time Electrochemical Impedance Spectroscopy (EIS) to estimate R_a and voltage degradation, enabling online RUL prediction during SOFC stack operation. Data-driven approaches, on the other hand, rely on trends in historical data rather than explicitly linking degradation to R_a. In [11], deep neural networks are used to predict the degradation trajectory and estimate the RUL. In [12], the authors integrate degradation evaluation into a prognostic framework and propose a data-driven method based on the voltage signal, decomposing and analyzing its components into trend and fluctuations.

Different methods have been explored so far, but a common factor across many studies is the use of Area Specific Resistance, R_a, estimation to predict the RUL of SOFCs.

978-1-6654-5771-2/25/$31.00 ©2025 IEEE

2025 6th International Conference on Control and Fault-Tolerant Systems (SysTol) | 978-1-6654-5771-2/25/$31.00 ©2025 IEEE | DOI: 10.1109/SYSTOL66549.2025.11267311

A limitation of these methods is the use of linear models for degradation drift, which can be an oversimplification as degradation is closely linked to the way the system is operated. Additionally, many approaches rely on large volumes of operational data or specific sensing systems that may not be suitable for real-time operation. When a full nonlinear model of degradation is available, as the one derived in [13], one interesting approach is Moving Horizon Estimation (MHE), which combines a dynamic model of the system with a finite window of past data, enabling real-time operation and constraint handling.

Contribution

This paper proposes a remaining useful life predictor for solid oxide fuel cells based on Moving Horizon Estimation. The estimator is developed using both the nonlinear model of the cell and of its degradation, then the estimated area specific resistance is used to determine the system's expected lifetime. The main contributions are summarized as follows:

Development of the MHE based on an extended reduced-order model of a SOFC, previously introduced by the authors in [14], incorporating both the cell's dynamic behavior and an experimental model for R_a degradation.

Design of a predictive framework that utilizes the estimated R_a together with its estimated rate of degradation, to provide both a minimum and an expected estimate of the cell's Remaining Useful Life (RUL).

Simulation results demonstrate the method's ability to accurately track the evolution of the cell's R_a over time.

II. System Modelling

In the following section, we present the SOFC dynamical and degradation models as presented in [14], first in their physical formulation, and later in state space.

Fig. 1 depicts a simplified scheme of a SOFC stack, highlighting the cells and the physical quantities of interest.

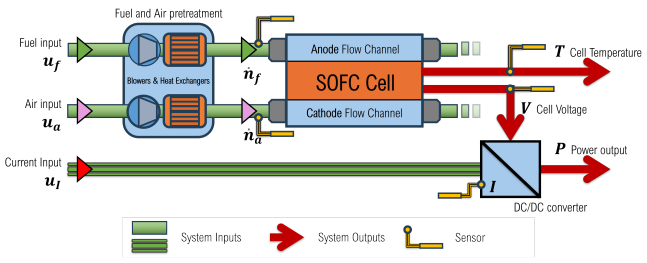

Fig. 1. Simplified scheme of a generic stand-alone SOFC system

A. Physical model of cell dynamics

The dynamical model of the cell employed in this work is the one introduced in [15] and [16]. It is a reduced order model of solid oxide fuel cell (SOFC-ROM). This formulation is zero-dimensional, assuming a constant temperature T throughout the cell.

At the anode of the cell, a preheated mixture of gases is supplied as fuel, at the cathode, preheated air is supplied. The main chemical reactions considered to occur inside the cell are methane steam reforming, the water-gas shift reaction, and the hydrogen oxidation reaction.

Before introducing the model, we clarify the notation: the subscript i refers to an individual chemical species in the fuel and the air streams, such that X_i represents the property X of the species i. When referring to a specific species, the subscript is explicitly specified, e.g., $X_{\mathrm{CH_4}}$ represents the property X of methane (CH_4). The subscript j designates the fuel f and air a streams, indicating that X_j represents the property X of the fuel, or of the air streams. The subscript m refers to a specific reaction, so that X_m represents the property X for reaction m. Finally, expressions with an overline (e.g., $\overline{X}$) denote constant values.

The dynamical equations are the following:

$$\frac{dT}{dt} = \Bigg(\underbrace{\sum_{i,j} \left(n_j \overline{K}_i h_i(\overline{T}_i) - \left(n_j \overline{K}_i + \textstyle\sum_m \overline{\nu}_{i,m} r_m\right) h_i(T)\right)}_{\text{Enthalpy Balance}} - \underbrace{IV}_{\text{Electric Power}} - \underbrace{\overline{\lambda}(T - \overline{T}_a)}_{\text{Heat Losses}} \Bigg) \frac{1}{\overline{c}_p} \tag{1}$$

$$V = \underbrace{-\frac{\Delta g}{2\overline{F}} + \frac{\overline{R}T}{2\overline{F}} \ln(Q)}_{\text{Nernst voltage}} - \underbrace{\frac{IR_a}{\overline{A}}}_{\text{Ohmic losses}} \tag{2}$$

The equation in (1) consists of the following components:

Enthalpy Balance: Here, T(K) denotes the internal temperature of the cell, n_j(mol/s) represents the molar flow rates of the fuel and air entering the system. The specific enthalpy of species i at temperature T is denoted by h_i(J/mol), and r_m(mol/s) denotes the reaction rate of reaction m. The constant $\overline{K}_i$(-) represents the concentration of species i within the molar flow n_j, $\overline{\nu}_{i,m}$(-) is the stoichiometric coefficient of species i in reaction m, while $\overline{T}_i$(K) is the constant inlet temperature of species i. The specific enthalpy h_i is calculated using the Shomate equation, with coefficients obtained from the National Institute of Standards and Technology (NIST) Chemistry WebBook [17]. The reaction rates r_m of the three reactions are chosen as in [15].

2. **Electric Power**: The second term in (1) represents the electrical power generated. In this term, I(A) denotes the current, and V(V) is the cell voltage, as expressed in (2).

3. **Heat Losses**: The final term represents the heat losses using Newton's cooling law, where $\overline{T}_a$ is assumed to be 25°C and $\overline{\lambda}$(J/s·K) is the heat transfer coefficient.

Equation (2) describes the cell voltage and it consists of the *Nernst Voltage* minus the *Ohmic losses* (in this ROM, various losses are simplified to a single Ohmic loss). In this expression, Δg(J/mol) represents the Gibbs free energy of the hydrogen oxidation reaction at temperature T, Q(-) is the reaction quotient (also from [16]), R_a, is the area specific resistance of the cell. Last $\overline{F}$(C/mol) is the Faraday constant, $\overline{R}$(J/mol·K) is the universal gas constant and $\overline{A}$(m²) is the active area.

B. Auxiliary Units Model

SOFCs are complex systems composed of a large number of components. Here we focus on the cell, assuming that the other components (e.g., blowers, heat exchangers, etc.) operate as expected. To account for the dynamics of these actuators, we model them as first-order low-pass filters for the three primary input variables: fuel flow n_f, air flow n_a, and current I. Their differential formulation is:

$$\dot{z}_j = -\frac{1}{\overline{\tau}_j} z_j + \frac{1}{\overline{\tau}_j} u_j \tag{3}$$

where $z_j = [n_f, n_a, I]$, is the input entering the physical system, $u_j = [u_f, u_a, u_I]$ is the control input and $\overline{\tau}_j$(s) is the associated time constant.

C. Area Specific Resistance Degradation Model

The R_a degradation model, commonly referred to as voltage degradation, is derived from the experimental observations reported in [18]. This formulation specifically describes the rate of increase in the cell's R_a ($\Omega{\cdot}\text{m}^2$), which contributes to ohmic losses in (2), which is given by the following differential equation:

$$\frac{dR_a}{dt} = \frac{\overline{k}_1 \mu_f + \overline{k}_2}{1 + e^{\frac{T - \overline{k}_3}{\overline{k}_4}}} \left(e^{\frac{\overline{k}_5 I}{A}} - 1 \right) \frac{R_a}{\overline{k}_0} \tag{4}$$

This expression describes the rate of change of R_a as function of the operating condition of the cell: temperature T, current I and fuel utilization μ_f (i.e., the fraction of fuel converted into electrical power [15]). First, R_a begins at a baseline value, representing a new, non-degraded cell. As time progresses, R_a increases whenever the cell is on. This cumulative effect models the aging process, capturing the decline in cell efficiency. The constants $\overline{k}_0, \ldots, \overline{k}_5$ are empirical and derived from long-term experiments [18].

III. Moving Horizon RUL Prediction

A. State Space Model

The state space formulation we introduce below is based on the physical models introduced before. The states are the differential variables T and R_a in (1) and in (4), and the inputs coming from the actuators as introduced in (3). The state vector x therefore defined as $x = \begin{bmatrix} T & R_a & n_f & n_a & I \end{bmatrix} \in \mathbb{R}^5$, the inputs vector is defined as $u = \begin{bmatrix} u_f & u_a & u_I \end{bmatrix} \in \mathbb{R}^3$.

Given this set of variables we can now define some functions that will be useful in the state space formulation:

$$\begin{aligned} f(x) = &\sum_{\substack{i \in \mathcal{S}, \\ j \in \mathcal{F}_x}} \left(x_j \overline{K}_i h_i(\overline{T}_i) - \left(x_j \overline{K}_i + \textstyle\sum_m \overline{\nu}_{i,m} r_m \right) h_i(x_1) \right) \\ &+ \overline{\lambda}(x_1 - \overline{T}_a) \end{aligned} \tag{5}$$

$$g(x) = -\frac{\Delta g}{2\overline{F}} + \frac{\overline{R} x_1}{2\overline{F}} \ln(Q) - \frac{x_5 x_2}{\overline{A}} \tag{6}$$

$$h(x) = \frac{\overline{k}_1 \mu_f + \overline{k}_2}{1 + e^{\frac{x_1 - \overline{k}_3}{\overline{k}_4}}} \left(e^{\frac{\overline{k}_5 x_5}{\overline{A}}} - 1 \right) \frac{1}{\overline{k}_0} \tag{7}$$

Function f includes the enthalpy balance and the heat losses in (1), function g represent the voltage expression in (2), and h is the gain of the degradation rate in (4). This leads us to the following state space formulation that merges the cell dynamics with the voltage degradation:

$$\dot{x} = \mathcal{F}(x, u) = \begin{cases} \dot{x}_1 = \dfrac{1}{\overline{c}_p} \left(f(x) - g(x)\, x_5 \right) \\ \dot{x}_2 = h(x)\, x_2 \\ \dot{x}_{3,4,5} = -\dfrac{1}{\overline{\tau}_{x_{3,4,5}}} x_3 + \dfrac{1}{\overline{\tau}_{x_{3,4,5}}} u_{1,2,3} \end{cases} \tag{8}$$

The output vector y includes temperature, voltage, current, and the inlet flow rates, and is defined as $y = \begin{bmatrix} T & V & n_f & n_a & I \end{bmatrix} \in \mathbb{R}^5$. Since in practice, the output variables y_i, $i \in \{1, \ldots, 5\}$, are obtained from physical sensors, it is reasonable to assume that each measurement is affected by noise. This can be modeled as:

$$y = \mathcal{G}(x) = \begin{cases} y_1 = x_1 + \eta_1 \\ y_2 = g(x) + \eta_2 \\ y_3 = x_3 + \eta_3 \\ y_4 = x_4 + \eta_4 \\ y_5 = x_5 + \eta_5 \end{cases} \tag{9}$$

Here, y_i represents the i-th measured output, and η_i is the corresponding measurement noise, zero-mean and bounded.

B. Moving Horizon Estimator

The proposed Moving Horizon Estimator (MHE) is implemented using the system in (8) and (9). The choice of the MHE formulation is motivated by its ability to handle nonlinearities, incorporate constraints, and leverage a sequence of measurements over time, which is particularly suitable for tracking slow-varying variables, such as degradation.

The continuous-time model is discretized using a standard fourth-order Runge-Kutta method. From this point on, the subscript k will denote the discrete time step, applying to states, inputs, and functions.

The MHE estimation problem is defined as follows:

$$\begin{aligned} \min_{\hat{x}_{k-N} \ldots \hat{x}_k} \quad & \sum_{i=0}^{N} \sum_{j=1}^{n_y} W_j^2 \left(y_{j,k-i} - \mathcal{G}_{k,j}(\hat{x}_{k-i}) \right)^2 \\ \text{s.t.} \quad & \hat{x}_{\tau+1} = \mathcal{F}_k(\hat{x}_\tau, u_\tau) \qquad \forall \tau \in [k{-}N,\, k{-}1] \\ & \overline{x}_{\min} \le \hat{x}_\tau \le \overline{x}_{\max} \qquad \forall \tau \in [k{-}N,\, k] \\ & \hat{x}_{2,k-N} = \psi_2 \quad \forall k \qquad \forall k \end{aligned} \tag{10}$$

Here, k is the current time instant, and N, the estimation horizon. The variable $\hat{x}_k = [\hat{x}_{k,1}, \ldots, \hat{x}_{k,5}]$ is the estimated state vector at time k, and the index $i \in \{0, \ldots, N\}$ denotes the backward time steps within the horizon. The measured outputs are denoted by $y_{j,k-i}$, where $j \in \{1, \ldots, n_y\}$ indexes the individual output components, with $n_y = 5$. The term $\mathcal{G}_{k,j}(\hat{x}_{k-i})$ corresponds to the model-computed output j using the estimated state $\hat{x}_{k-i}$ and equation (9). Each output error is weighted by a corresponding factor W_j.

The objective function (10) minimizes the difference between the measured and predicted outputs in the horizon. The solution provides the sequence of estimates $\hat{x}_{k-N} \ldots \hat{x}_k$ that best fit the measurements while satisfying the constraints.

The next three terms represent the constraints. The first ensures that the estimated states evolve according to the nonlinear model dynamics, defined in (8). The second constraint imposes bounds on the states, defined by $\overline{x}_{\min}$ and $\overline{x}_{\max}$, which reflect physical limitations and operational boundaries.

The third constraint is introduced to improve the consistency of R_a estimation (i.e., $\hat{x}_2$). Here, ψ_l, with $l = 1, .., N$ is the estimated vector $\hat{x}_2$ in the previous horizon. This means that ψ_2 is equal the second value of the estimated R_a computed in the previous iteration. Since R_a has a very small drift, it is easy for the estimator to fit a solution which may be uncorrelated with the previous. However, since our main goal is to track the overall drift of R_a, we introduce this constraint that links the first estimated value of the new horizon $\hat{x}_{k-N}$ to the second estimated value of the previous horizon $\psi_{2,k-N}$. This ensures that the overall drift of the resistance will remain consistent. For the initial guess of the estimator, it is crucial to provide an accurate estimate of R_a, since this constraint propagates any potential initial bias.

C. Remaining Useful Life Prediction

Once the MHE problem is formulated and provides a real-time estimate of R_a (i.e., $\hat{x}_2$), it is possible to define a predictor for the cell's RUL. The core idea is that the system has a maximum tolerable value of R_a, denoted as $\overline{R}_{\text{EoL}}$, beyond which the cell is considered to be at the End of Life (EoL) due to excessive degradation. The specific criterion for defining EoL can vary. For example, as cited in [8], EoL may be defined as a 10% drop in output voltage.

Based on this threshold and the estimated state vector $\hat{x}$ at time k, we compute two RUL estimates: RUL_{min} a conservative lower bound, and RUL_{avg} a nominal estimate. First, we initialize two parameters to zero: $\dot{\hat{x}}_2^{\text{max}}$, the maximum estimated degradation rate, and $\dot{\hat{x}}_2^{\text{avg}}$, the average estimated degradation rate. Then, at each k, we perform:

1) Collect $\hat{x}_k$ from the MHE and compute $\dot{\hat{x}}_{2,k}$ using (4).
2) If $\dot{\hat{x}}_{2,k} > \dot{\hat{x}}_2^{\text{max}}$, update: $\dot{\hat{x}}_2^{\text{max}} \leftarrow \dot{\hat{x}}_{2,k}$
3) Update the average degradation rate: $\dot{\hat{x}}_2^{\text{avg}} \leftarrow \frac{(k-1)\dot{\hat{x}}_2^{\text{avg}} + \dot{\hat{x}}_{2,k}}{k}$
4) Compute the conservative RUL estimate: $\text{RUL}_{\text{min}} \leftarrow \frac{\overline{R}_{\text{EoL}} - \hat{x}_{2,k}}{\dot{\hat{x}}_2^{\text{max}}}$
5) Compute the nominal RUL estimate: $\text{RUL}_{\text{avg}} \leftarrow \frac{\overline{R}_{\text{EoL}} - \hat{x}_{2,k}}{\dot{\hat{x}}_2^{\text{avg}}}$

This simple algorithm allows us to update in real time the RUL prediction, as new data becomes available.

IV. Simulation Results

In this section, we present the simulation results. The parametrization of the SOFC used in the simulations follows the model in [15], which is based on an off-the-shelf cell, and the experimental degradation model in [13]. The SOFC is regulated using a dynamic tracking controller previously developed. The main objective of the controller is to track a given power profile while maintaining a constant temperature setpoint. In this study, we adopt a square-wave power profile to alternate between high (i.e., accelerated degradation) and low power demands (i.e., reduced degradation). The MHE

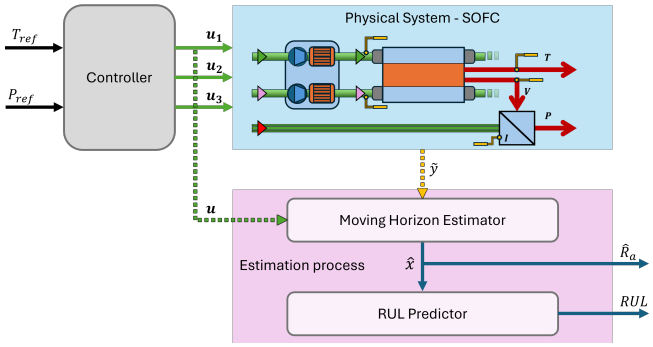

Fig. 2. Block diagram of the setup, including the controller (gray), the SOFC (light blue), and the estimator with the RUL predictor module (pink).

receives noisy measurements $\tilde{y}$ from the cell along with the control inputs applied by the controller u, and computes the state estimate $\hat{x}$ at each time step k. Once the estimated state vector $\hat{x}$ is obtained, it is passed to the RUL predictor, which evaluates the remaining useful life using the metrics RUL_{min} and RUL_{avg} according to the steps in III-C. The overall scheme is illustrated in Figure 2.

TABLE I
REFERENCE VALUES, CONSTRAINTS AND PARAMETERS

Reference	
Objective	**Details**
Temperature Tracking	T_{ref}: 1100 K, constant
Power Tracking	P_{ref}: Square Wave 10-17 W, 500 s cycle
MHE problem constraints	
Description	**Constraint**
Temperature $\hat{x}_1$	$973\,\text{K} \leq T \leq 1133\,\text{K}$
Fuel flow $\hat{x}_3$	$0 \leq \hat{x}_3 \leq 5 \times 10^{-4}$ mol/s,
Air flow $\hat{x}_4$	$0 \leq \hat{x}_4 \leq 3 \times 10^{-3}$ mol/s,
Current $\hat{x}_5$	$0\,\text{A} \leq \hat{x}_5 \leq 30\,\text{A}$
Parameters	
Description	**Details**
Timestamp T_s	10 s
Horizon length N	10, 25, 50 steps
Initial $x_2(0)$	$1 \times 10^{-4}\ \Omega\,\text{m}^2$
R_a threshold $\overline{R}_{\text{EoL}}$	$x_2(0) \times (1 + 0.25\,‰)$
Cost function weights W	$[1,\ 1,\ 1,\ 1,\ 1]$
Measurement noise η	Zero-mean white noise. Standard deviation for each signal is computed as a fixed percentage of its nominal value: $\eta = \overline{y}_{\text{nom}} \cdot [0.5,\ 1,\ 5,\ 5,\ 0.7] \times 10^{-3}$
Nominal values $\overline{y}_{\text{nom}}$	$[1100\text{K}, 0.7\text{V}, 2.05 \times 10^{-4}\text{mol/s}, 1.8 \times 10^{-3}\text{mol/s}, 15\ \text{A}]$

The simulations were performed in the MATLAB environment using the CasADi software library. The main parameters of the simulation setup are summarized in Table IV. The table includes the controller's objective, the definition of the operational constraints of the SOFC, and parameters. Two important considerations should be noted: first, the noise levels were selected to reflect typical uncertainties observed in high-end sensors; second we opted for a uniform

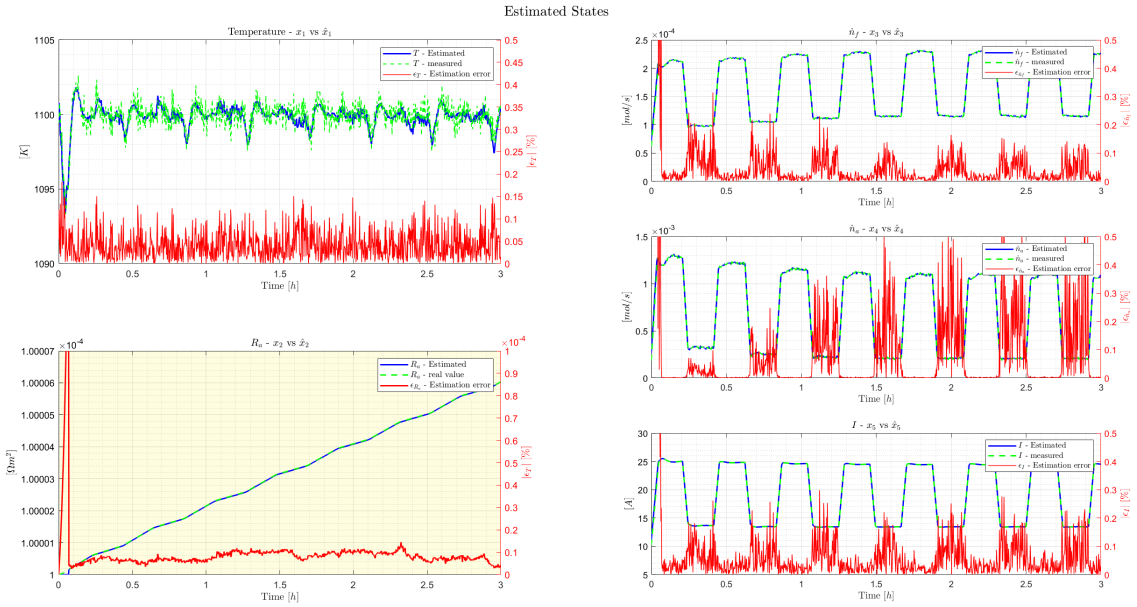

Fig. 3. MHE estimated states for $N = 25$. The estimated states $\hat{x}$ are shown in solid blue, the measured values are represented by green dashed lines. The red curve indicates the absolute relative estimation error between the predicted and measured states, and its in % of the nominal value.

TABLE II

ESTIMATION ERRORS FOR DIFFERENT HORIZON LENGTHS

State	N = 10		N = 25		N = 50	
	MAE	RMSE	MAE	RMSE	MAE	RMSE
$\hat{x}_1$ (T)	0.050	0.107	0.041	0.051	0.039	0.049
$\hat{x}_2$ (R_a)	8.45e-6	9.10e-6	7.89e-6	8.14e-6	8.06e-6	3.99e-5
$\hat{x}_3$ (n_f)	0.051	0.228	0.038	0.056	0.051	0.129
$\hat{x}_4$ (n_a)	0.113	0.807	0.063	0.128	0.070	0.155
$\hat{x}_5$ (I)	0.064	0.225	0.053	0.075	0.055	0.079

weighting W since the measurement noise are of similar magnitude and do not justify strong differentiation. Last, since degradation manifests its effects over thousands of hours, a comparatively small value for $\overline{R}_{EoL}$ was chosen. This decision was made to demonstrate the potential of the method in a short simulation time.

In Figure 3, the main results of the MHE are presented for a horizon $N = 25$, while Table II offers a comparison of the prediction errors for different horizon lengths. Despite using equal weighting factors W, the overall estimation performance is good, with the absolute relative percentage error consistently below 0.5% for all estimated states. Notably, for $\hat{x}_2$, the estimated R_a, the error is even smaller, on the order of 10^{-5}. This is primarily due to two factors: first, the accurate initial value for $R_a(0)$, and second, the consistent estimation of the degradation rate over time. Other estimation setups, initialized with different R_a values, yielded similar results regarding drift. However, due to the continuity constraint introduced in (10), the magnitude of the error is inherently tied to the accuracy of the initial guess.

Looking at the results in Table II, the mean absolute error (MAE) and the root mean square error (RMSE) are computed with respect to the true value over the entire simulation. Here we observe that increasing the horizon improves the overall performance from 10 to 25 steps. However, extending the horizon to 50 steps does not reduce the error. This may be due to the fact that we included only sensor noise, while there is no uncertainty in our model, therefore the accumulation of measurement noise may dominate for longer horizons.

The results of the RUL prediction are shown in Figure 4. The blue line represents the estimated value of $\hat{x}_2$, while the red line indicates the threshold $\overline{R}_{EoL}$. The green dashed and pink dotted lines illustrate the projections of the average and maximum degradation rates, $\hat{\dot{x}}_2^{\text{avg}}$ and $\hat{\dot{x}}_2^{\text{max}}$ respectively, from the current time to their intersection with the $\overline{R}_{EoL}$ threshold. The minimum RUL indicates the shortest time required to reach the threshold, assuming the maximum estimated degradation rate, which in our case is $\text{RUL}_{\text{min}} \sim 6h$. The average RUL, less conservative, is based on the average rate of degradation, and in this case is $\text{RUL}_{\text{avg}} \sim 10h$.

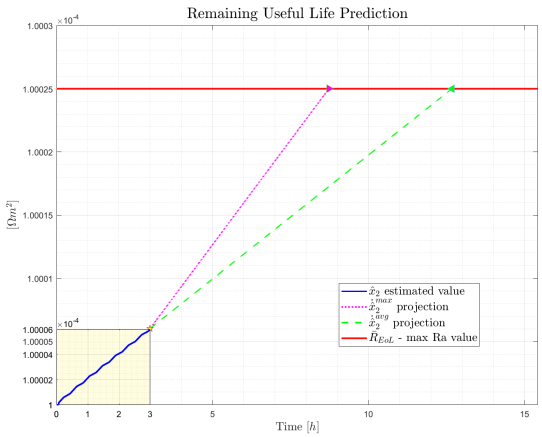

Fig. 4. RUL prediction at the end of the simulation. The area highlighted in yellow correspond to the highlighted area in figure 3.

In summary, the simulation results demonstrate the ability

of the MHE to accurately estimate the state vector $\hat{x}$, and to track the drift of R_a in real time. The degradation rate is on the order of 10^{-14}, and the overall increase in R_a after 3 h of operation is approximately $5 \times 10^{-9} \Omega m^2$, making the performance particularly remarkable considering the scale. However, it is important to acknowledge that a good initial guess for $\overline{R}_a(0)$ is essential to achieve these results. In parallel, the predictor was able to provide an interval for the RUL, using the minimum expected RUL based on the maximum degradation rate, as well as the expected RUL based on the average degradation rate. As time progresses, the average expected RUL becomes more accurate and converges to a value that reflects the actual operating conditions of the cell, while the minimum RUL remains a conservative bound, considering the most stressful operating scenario.

V. Conclusion

In conclusion, this work contributes to the field of Solid Oxide Fuell Cells (SOFCs) internal state and remaining useful life estimation by proposing a moving horizon approach capable of estimating both measured and unmeasured states of the cell, along with an interval prediction of its remaining useful life. Such methods are crucial for the broad adoption of SOFC technology in the marine industry, especially in light of the ongoing decarbonization efforts of the sector.

The proposed method operates in two stages: first, the moving horizon estimator is used to estimate the full system state, including the area-specific resistance, using a nonlinear extended state space model of the cell introduced in a previous work. Estimating the area-specific resistance is particularly challenging due to two factors: its degradation occurs over thousands of hours, and its rate depends nonlinearly on the system states, making it coupled with the system dynamics and prone to noise. In the second stage, this estimate is used to recursively compute both the average and minimum remaining useful life of the cell, by extrapolating the average and maximum degradation rates. By projecting these two rates into the future, the remaining useful life indicators are predicted based on when a predefined threshold is reached. These indicators provide operators with insight into both the expected degradation trend and the worst-case scenario, allowing for more informed decision-making.

Future work will focus on enhancing the robustness of the proposed method against uncertainties such as sensor noise and model mismatches. For instance, the initial value of the area-specific resistance, which may not be precisely known. Another field of interest is the integration of the estimated state vector into the control loop, enabling the controller to account for the current drift in area-specific resistance. This would support accurate power tracking even under significant degradation and enable degradation-aware operation. Such improvements would enhance the management of SOFC operational lifetime and support integration with maintenance planning, facilitating the widespread adoption of these technologies in the maritime sector and other applications.

References

[1] R. Maric, *Solid Oxide Fuel Cells: From Fundamental Principles to Complete Systems*, 1st. CRC Press, 2020. DOI: 10.1201/9780429100000.

[2] International Maritime Organization, *Cutting greenhouse gas emissions*, 2023. [Online]. Available: https://www.imo.org/en/MediaCentre/HotTopics/Pages/Cutting-GHG-emissions.aspx.

[3] S. C. Singhal and K. Kendall, *High-temperature Solid Oxide Fuel Cells: Fundamentals, Design and Applications*. Elsevier, 2003, pp. 1–405.

[4] J. Milewski and J. Lewandowski, "Comparative analysis of time constants in solid oxide fuel cell processes–selection of key processes for modeling power systems," *Journal of Power Technologies*, vol. 91, pp. 1–5, 2011.

[5] H. Yokokawa, H. Tu, B. Iwanschitz, and A. Mai, "Fundamental mechanisms limiting solid oxide fuel cell durability," *Journal of Power Sources*, vol. 182, pp. 400–412, 2008.

[6] S. Zarabi Golkhatmi, M. I. Asghar, and P. D. Lund, "A review on solid oxide fuel cell durability: Latest progress, mechanisms, and study tools," *Renewable and Sustainable Energy Reviews*, vol. 161, p. 112 339, 2022.

[7] T. Skafte, J. Hjelm, P. Blennow, and C. Graves, "Quantitative review of degradation and lifetime of solid oxide cells and stacks," in *Proceedings of the 12th European SOFC & SOE Forum*, Jul. 2016, B0501.

[8] B. Dolenc, P. Boškoski, M. Stepančič, A. Pohjoranta, and Juričić, "State of health estimation and remaining useful life prediction of solid oxide fuel cell stack," *Energy Conversion and Management*, vol. 148, pp. 993–1002, 2017.

[9] L. Cui, H. Huo, G. Xie, J. Xu, X. Kuang, and Z. Dong, "Long-term degradation trend prediction and remaining useful life estimation for solid oxide fuel cells," *Sustainability (Switzerland)*, vol. 14, no. 15, 2022.

[10] M. Gallo, P. Polverino, J. Mougin, B. Morel, and C. Pianese, "Coupling electrochemical impedance spectroscopy and model-based aging estimation for solid oxide fuel cell stacks lifetime prediction," *Applied Energy*, vol. 279, p. 115 718, 2020.

[11] S.-J. Cheng, W.-K. Li, T.-J. Chang, and C.-H. Hsu, "Data-driven prognostics of the sofc system based on dynamic neural network models," *Energies*, vol. 14, no. 18, 2021.

[12] X. Zhang, Z. He, Z. Zhan, and T. Han, "Performance degradation analysis and fault prognostics of solid oxide fuel cells using the data-driven method," *International Journal of Hydrogen Energy*, vol. 46, no. 35, pp. 18 511–18 523, 2021.

[13] V. Zaccaria, D. Tucker, A. Traverso, P. Pezzini, and K. M. Bryden, *Active Control of Fuel Cell Degradation in an SOFC/GT Hybrid System*, Jun. 2017.

[14] A. Caspani, R. R. Negenborn, and V. Reppa, "Degradation-conscious model predictive control for marine solid-oxide fuel cells," in *Proceedings of the European Control Conference (ECC)*, Accepted, to appear, 2025.

[15] L. van Biert, P. S. Castillo, A. Haseltalab, and R. R. Negenborn, "A reduced-order model of a solid oxide fuel cell stack for model predictive control," in *Proceedings of the International Ship Control Systems Symposium*, 2022.

[16] L. van Biert, M. Godjevac, K. Visser, and P. Aravind, "Dynamic modelling of a direct internal reforming solid oxide fuel cell stack based on single cell experiments," *Applied Energy*, vol. 250, pp. 976–990, 2019.

[17] P. J. Linstrom, W. G. Mallard, N. I. of Standards, and T. (U.S.), *Nist chemistry webbook*, Aug. 1997 release, 1997.

[18] V. Zaccaria, D. Tucker, and A. Traverso, "A distributed real-time model of degradation in a solid oxide fuel cell, part i: Model characterization," *Journal of Power Sources*, vol. 311, pp. 175–181, 2016.